Flow Turbulence Combust (2016) 97:451–474
DOI 10.1007/s10494-016-9707-8

Scour Hole Influence on Turbulent Flow Field around Complex Bridge Piers

A. A. Beheshti[1] · B. Ataie-Ashtiani[2]

Received: 17 April 2014 / Accepted: 12 January 2016 / Published online: 2 February 2016

Abstract Experimental results of detailed flow measurements using an Acoustic-Doppler Velocimeter (ADV) around a complex bridge pier (CBP) are presented. The pier consists of a column, a pile cap (PC) and a 2×4 pile group. The time-averaged velocities, turbulence intensities, and Reynolds stresses are studied and presented at different horizontal and vertical planes. Streamlines obtained from the velocity fields are used to show the complexity of the flow around the pier. It is shown that the main feature of the flow responsible for the entrainment of the bed sediments is a contracted (pressurized) flow below the PC toward the piles. A deflected flow around the PC and a strong down-flow along its sides are observed and have been measured. It is shown that these flow patterns also cause sediment entrainment. Vortex flow behind the PC and amplification of turbulence intensity along its sides near the downstream region can be other reasons for the scour hole (SH) development. Turbulence intensities and Reynolds shear stresses are presented and discussed. A comparison is made between the flow field measured with the equilibrium SH and that measured on the fixed flat-bed. The results show that the flow field around the PC is considerably influenced by the development of the SH. The extent of the wake region at the rear of the PC is about 1.4 times larger for the fixed bed (FB) than for the scoured bed (SB). Moreover, the size of the core of high turbulent kinetic energy K, as well as the maximum values of K behind the column for the FB case is larger than that of the SB case. When a scour hole develops, the flow below the PC around the piles is considered to be the main cause of the scour. This is

✉ A. A. Beheshti
beheshti@ferdowsi.um.ac.ir

B. Ataie-Ashtiani
ataie@sharif.ir

[1] Water Resources Engineering Department, Ferdowsi University of Mashhad, P.O.Box 91775-1163, Mashhad, Iran

[2] Civil Engineering Department, Sharif University of Technology, P.O.Box 11155-9313, 66164236, Tehran, Iran

the first time that these observations about the flow and turbulence field around a complex bridge pier are reported and analyzed. In addition to improving the understanding of the flow structure, the present detailed measurements can also be used for benchmarking and verification of numerical models.

Keywords Bridge foundation · Complex pier · Physical modeling · Scour hole · Turbulent flow

1 Introduction

Numerous investigations have been performed to understand the flow and erosion mechanisms around bridge foundations and to estimate the scour depth [1–5]. Using these studies, some empirical relations were presented for the prediction of local scour depth around bridge piers [1–3]. The application of existing relations to complex flow patterns is problematic and often leads to questionable results in field applications [6] or even for laboratory conditions [7, 8]. Lack of understanding of the flow field and erosion mechanisms seems to be at least partly responsible for this state. Comprehensive understanding of the turbulent flow fields aids the accurate prediction of the scour magnitude [9]. In the past, the turbulent flow around a bridge pier with and without a scour hole (SH) has been studied both computationally and experimentally [4, 5, 7, 10, 11]. Dargahi [4] reported the result of several studies that focused on the visualization of the vertical structures around a bridge pier placed in an incoming fully turbulent flow at different stages of the scour process. Ahmed and Rajaratnam [10] studied the flow past cylindrical piers on smooth, rough and mobile beds. Their study focused on the flow in the symmetry plane and the effect of bed roughness and SH on this flow. Graf and Istiarto [11] measured the mean velocity components and turbulent Reynolds stresses using an ADV profiler in several planes around a circular pier for equilibrium scour conditions. Roulund et al. [12] performed visualizations of the flow in the SH during the evolution of the scour process and measured flow field and bed shear stresses for circular bridge piers on a flat bed (FB). Dey and Raikar [9] studied experimentally the structure of the turbulent horseshoe vortex flow within the developing SHs at cylindrical piers by measuring instantaneous 3D velocities using an ADV. However, in their work the flow in the wake of the pier was not studied; they concluded that the flow and turbulence intensities in the horseshoe-vortex remain rather similar during the development of the SH. Kirkil et al. [5] performed comprehensive Large-eddy simulations (LES) and laboratory-flume visualizations of the flow in a SH around a circular cylinder. They used the LES results together with flow visualizations using dye and Large Scale Particle Image Velocimetry (LSPIV) techniques to educe the coherent structures around a cylinder located in a SH. Kirkil and Constantinescu [13] investigated the mechanisms driving the bed erosion during the advanced stages of the scour process around an in-stream rectangular cylinder using experimental measurements and Detached Eddy Simulations. Ataie-Ashtiani and Aslani-Kordkandi [14, 15] analyzed the ADV measurements of turbulent flow field around single, side-by-side and tandem pile groups with and without a SH. They showed that the presence of a SH changes the behavior of vortex shedding considerably for their rather simple pier set-up.

Despite a rapidly expanding body of literature on the flow and scour around cylindrical piers, there remain challenges for flow field description and estimating design scour depths

around piers with complex shapes. Due to geotechnical and economical reasons, bridge designs often lead to a complex foundation [8, 16, 17] and most of the large bridge piers are complex in shape and consist of several clearly definable components [18].

Previous studies have shown that the existing methodologies for predicting local scour depth at complex bridge piers (CBPs) do not provide credible predictions of scour depth in some cases [16–18]. Accurate prediction of scour pattern around pier foundations strongly depends on resolving the flow structure and the mechanism of sediment movement around the pier. The continuous advances in computer power and numerical techniques allowed sophisticated simulations of the unsteady velocity fields to be obtained in recent years. Significant progress in this direction has been achieved by simulations of unsteady laminar flow [19], and simulations of unsteady turbulent flow [20]. However, owing to the complexity of the geometry and flow, these simulations often have limitations so that further refinement and verification are necessary. To the best of our knowledge, few studies have examined the flow and turbulence field around CBPs. Ge and Sotiropoulos [21] developed an unsteady, fully 3D numerical method for solving unsteady Reynolds-averaged Navier-Stokes (URANS) equations for real-life bridge foundation geometries. Ge et al. [20] validated and applied this model to investigate the physics of flow past a complex real-life bridge foundation mounted on a flat bed (FB). They compared the results of experimental measurements of mean velocity and turbulence kinetic energy profiles with the numerical simulations and showed that there exists good agreement between the results. In addition, the computed flat-bed flow characteristics were analyzed in comparison with the scour patterns observed in the laboratory to identify key flow features responsible for the initiation of scour. In an earlier study by the authors [22], the turbulent flow field around a CBP located on a rough FB was carefully studied by measuring instantaneous velocities. More recently Kumar and Kothyari [23] conducted experiments on the flow pattern and turbulence characteristics around a circular uniform pier and a compound pier (consisting of a circular pier of diameter 114 mm with a circular footing of diameter 210 mm) in the presence of a SH using an ADV. They found that the diameter of the principal vortex upstream of the compound pier is 1.11 and 0.85 times as large as that for the circular uniform pier, when the top surface of the footing was above and below the general channel bed level, respectively.

Existing studies of the flow field around CBPs are limited to fixed flat-bed cases. However, the presence of a SH may alter both the structure of the flow and the intensity of the vortical structures obtained for flat-bed cases [14, 15]. Therefore, the validity of numerical models has also to be evaluated for situations in which a SH is present. To the authors' knowledge, studies on the flow around CBPs with the presence of a SH have not been published yet. The present study attempts to fill this gap.

The primary objective of the present study is to provide a comprehensive data set for the mean flow and turbulence characteristics for the case of a particular CBP located in a SH under equilibrium conditions. The data set enhances the three-dimensional flow structure understanding for CBPs. The interactions between pier elements and their effects on the flow field have not been studied yet. We will address how the flow and turbulence characteristics change in the equilibrium SH around a CBP, by comparing the measured flow field with that of the FB case. Additionally, the paper aims at providing a benchmark experimental data set as a resource for the validation of 3D computational fluid dynamics codes that utilize a free-surface model. It is expected that these new observations on the flow structure will be useful for scour modeling around complex piers and will be helpful in the design process.

2 Experimental Setup and Velocity Measurements

The experiments were conducted in a rectangular test channel 15 m long, 1.26 m wide, and 0.9 m deep. For the experimental work, a false floor was made on the bottom of the channel. A CBP was placed in a sediment recess 2 m long, 1.26 m wide, and 0.35 m deep, which was filled with uniform sand of median diameter, d_{50} of 0.71 mm, specific gravity, S_s of 2.45 and geometric standard deviation, σ_g of 1.20. The sediment recess was located at a distance 10 m from the upstream end of the channel. The CBP used in the experiments consisted of a column, a pile cap (PC) and a 2×4 pile group (Fig. 1). For the CBP selected in this study, all elements are exposed to the approaching flow. This situation occurs frequently when bridges have a complex foundation [16]. The approach flow depth, h, was maintained as 0.301 m; and the depth-averaged approach flow velocity U_0 was set as 0.358 m/s, which was about 97 % of the critical velocity of the uniform sand bed to satisfy the clear water condition. The critical bed shear velocity was calculated using the method proposed by Beheshti and Ataie-Ashtiani [24]. The critical Shields parameter τ_{*c} is calculated as $\tau_{*c} = u_{*c}^2/(\Delta g d) = 0.025$ and the undisturbed Shields parameter is $\tau_* = 0.024$, where u_* is the friction velocity, $\Delta = (\rho_s - \rho)/\rho$, g is the gravitational acceleration, d the particle diameter, ρ_s the particle density and ρ the fluid density. Table 1 summarizes the parameters of the CBP geometry and the flow and sediment conditions tested. In this table, D_c is the column width, L_c is the column length, D_{pc} is the PC width, L_{pc} is the PC length, T is the PC thickness, Y is the distance from the initial bed level to the top of the PC, b_p is the diameter of the piles in the foundation, G is the side to side distance between the piles, n is the number of piles normal to the flow direction, and m is the number of piles in line with the flow. The test conditions (except flow conditions) are similar to those used in a previous study with a flat bed (FB) reported by Beheshti and Ataie-Ashtiani [22].

To measure the flow field in the equilibrium SH case, the experiment was first run for a period of 72 h starting from a flat bed. During this experiment, the bed changes in front of the PC were measured using ADV. It was observed that for the pier studied here, scour depth development was negligible after 48 h. However, the total duration of the run was adequate for achieving equilibrium scour at the CBP for which the PC position was above the initial bed level [17]. After the run was stopped, the column and PC were removed and the scour depth was carefully measured by a Vernier point gauge. The contour lines of the SH around the CBP are shown in Fig. 2. The maximum equilibrium scour depth d_{se}, located at the inner sides of the first piles, was measured as 0.155 m.

To facilitate measurements by ADV, the water was first drained out and then, when the bed was dry, a synthetic resin was sprayed uniformly over the SB to fix it, as was done by Dey and Raikar [9] and Beheshti and Ataie-Ashtiani [22]. The flow was then established again for the fixed SB situation and the instantaneous three-dimensional velocity components were measured by a NorTek made 5 cm ADV [25]. The ADV operated on a pulse-to-pulse coherent Doppler shift to provide instantaneous three-dimensional velocity components at a rate of 25 Hz. The ADV has relatively low flow-field interference as the measurement location is 5 cm below the probe. Velocity measurements with the ADV down-looking probe were not possible in the zone located 5 cm below the free surface, so an up-looking probe was used to measure the flow in this region. The measurements in this experiment were taken in the Cartesian coordinate system (x, y, z) with time-averaged velocity components (u, v, w) and fluctuation components (u', v', w'), respectively. The coordinate $x$is defined as the distance from the leading edge of the column, y is the transverse distance from the center line (line of symmetry) of the pier, and $z$is the vertical distance from the initial bed level. A negative $x$value refers to a section located upstream of the

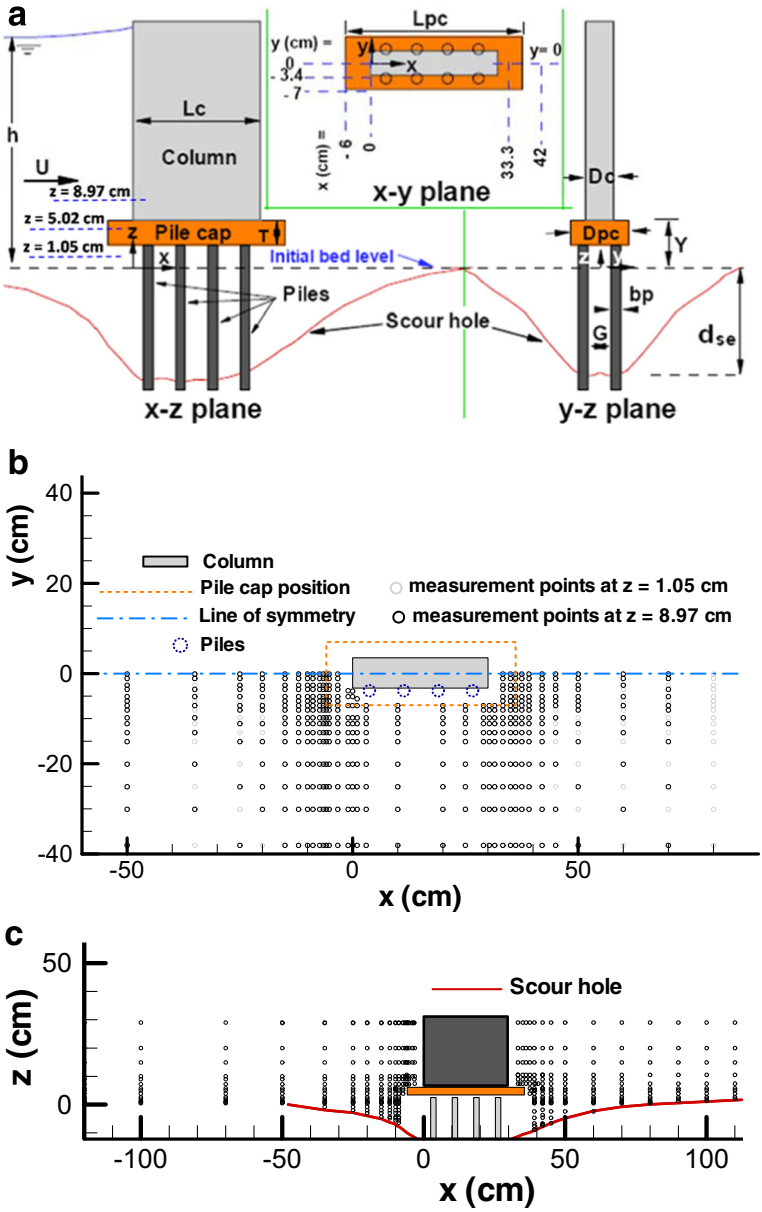

Fig. 1 **a** Complex pier used in experiments: definition of geometrical parameters; **b** locations of measurement points in horizontal planes; **c** locations of measurement points at vertical section y = 0

leading edge of the column (Fig. 1). The measurements were carried out at the mid-span of the CBP (y<0) and the results are available on one side of the centerline (y <0). Measurements in horizontal planes (z= 1.05, 5.02, and 8.97 cm from bed) were taken at several points [Fig. 1b]. Moreover, at vertical sections y = 0, -3.4, and -7 cm and x= -6, 0, 33.3

Table 1 Flow, sediment, and complex pier characteristics used in experiments

n×m	G/b_p	b_p(cm)	Y (cm)	T (cm)	L_{pc}(cm)	D_{pc}(cm)	L_c(cm)	D_c(cm)	u_*/u_{*c}	d_{50} (mm)	U (m/s)	h (cm)
2×4	3	2.54	6.15	3.36	42	14	30.3	6.8	≈ 0.97	0.71	0.358	30.1

and 42 cm [Fig. 1a(x-y plane)], the ADV readings were taken at different vertical positions [Fig. 1c]. At a total of 2742 points, velocity measurements were made. Moreover, measurements were made at an upstream location x = -120 cm. Figure 3 shows the mean streamwise velocity profile (Fig. 3a) and turbulent kinetic energy profile (Fig. 3b) defining the approach flow. The velocity components of v and w were nearly zero at this point. According to Fig. 3a, a fully developed turbulent flow was attained as approach flow to the test section. Depending on the measurement point and turbulence intensity (TI), the sampling duration was 120–300 s in order to obtain a statistically time-independent average velocity. It is noted that ADV measurements at points closer than about 3.5 cm to the pier were not possible. The instruments, measurement techniques, and method of analysis used in this study are the same as those in Beheshti and Ataie-Ashtiani [22] and hence the details are not provided here again.

2.1 Data analysis

Prior to data processing, each record was visually inspected to identify possible problems such as spikes, trends, or abrupt discontinuities in the velocity time series. By inspection of velocity time series measured with the ADV it was found that there is a zone located between 2.9 and 3.8 cm above the local bed where signal quality decreased sharply and turbulent fluctuations are not realistic. Inspection of turbulent kinetic energy (K) profiles facilitated the identification of these points. The data collected at such points were not included in the analysis. This study also found that the velocity and turbulence measurements at some points suffered from the same noise problems experienced by other investigators, especially in the regions that experienced high turbulence levels. All velocity records were processed using the public domain software WinADV [26] to obtain the time mean and RMS (root mean square) values of each point velocity record. Measurements were filtered using WinADV to reject points with a correlation coefficient less than 0.70 and signal to noise ratio less than 15. Also, output data from ADV was filtered using the spike removal algorithm after Wahl [27]. The time series inspection and stationarity analysis confirm that the obtained time series were long and stationary enough to accurately define turbulence characteristics. Using the spectral analysis method of Voulgaris and Trowbridge

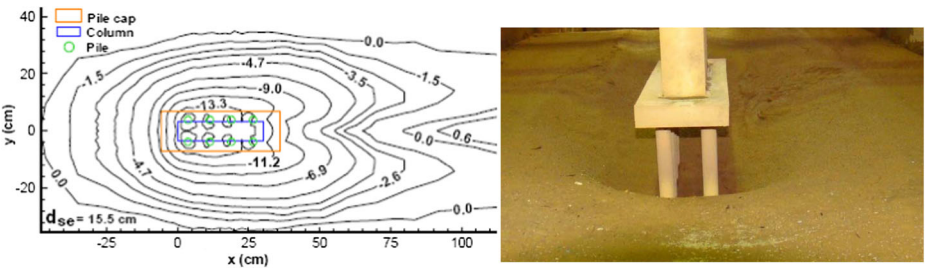

Fig. 2 Scour contours (*left*) and bathymetry at equilibrium conditions (*right*) around the complex pier

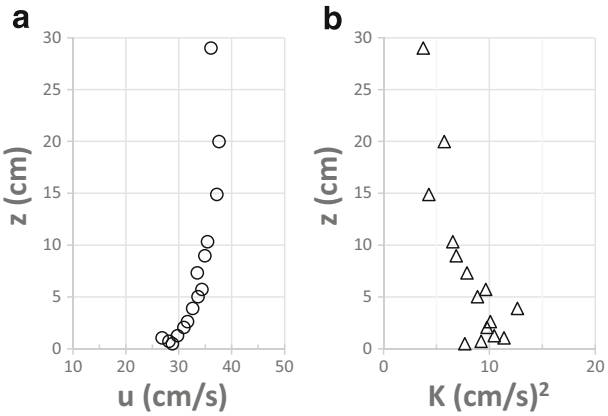

Fig. 3 Profiles of streamwise velocity u (**a**) and turbulent kinetic energy K (**b**) at an upstream station located at x = -120 cm

[28] and the method proposed by García et al [29] for detection of the Doppler noise energy level, it was shown that the highest ratio of relative importance of the noise energy over the real turbulent energy could be about 7 % for velocity measurements.

The corrected velocity data were used to calculate the following statistical quantities: (1) Mean velocities (u, v, w); (2) turbulent fluctuation velocities ($u^+ = (\overline{u'u'})^{0.5}$, $v^+ = (\overline{v'v'})^{0.5}$, $w^+ = (\overline{w'w'})^{0.5}$) as the standard deviations of the measurements of the instantaneous velocities; (3) Reynolds shear stresses (RSSes) including $\overline{u'v'}$, $\overline{u'w'}$, $\overline{v'w'}$; and (4) total turbulence energy $K = 0.5(\overline{u'u'} + \overline{v'v'} + \overline{w'w'})$.

3 Results and Discussions

3.1 Mean flow

In the following sections, measurements are presented as streamlines and velocity contours at different sections. A limited number of plots have been provided in this section. More results including contour plots and streamlines are available as Supplementary files that can be obtained at request from the first author.

3.1.1 Flow pattern in vertical symmetry plane

Contour plots of the streamwise (u) and vertical (w) velocity in the vertical symmetry plane y=0 for both scoured bed (SB) and fixed bed (FB) cases are shown in Figs. 4 and 5, respectively. Moreover, the streamlines in this plane are shown in Fig. 6 with blow-ups in the downstream (near wake) region. In the upstream region, the streamwise velocity approaching the pier decreases due to the effect of velocity reduction in front of the PC and the column (Fig. 4a). Vertical changes of u show that it's magnitude increases with distance from the bed up to an elevation near the PC and then it decreases approaching the region of decelerating flow in front of the PC (see Fig. 4a). The contours of w in the vertical symmetry plane depicted in Fig. 5 show that toward the pier the flow is deflected in the vertical direction at the front of the PC, with an upward flow toward the column and a contracted downward flow below the PC toward the piles. The maximum magnitude of w found at

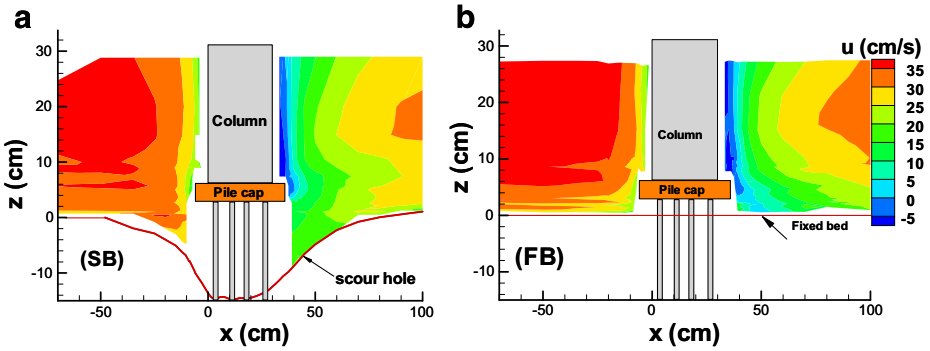

Fig. 4 Velocity contours of u component in the vertical symmetry plane y=0 for SB (**a**) and FB (**b**) cases

any of the measurement points was about -0.31U_0 near the upstream edge of the PC (see Fig. 5a). Figures 4 and 6 show that, in contrast to the findings for a cylindrical pier [9], upstream of the pier and at measured points in the SH, reverse flow that would indicate a horseshoe vortex was not measured. This can be attributed to the fact that the flow near the bed is only little obstructed by the piles and can pass in the gap underneath the PC or through the scour hole in the SB case.

Downstream of the pier, the flow is first dominated by separation at the PC and column. However, no reverse flow was observed in the region below the pile cap position because of through flow underneath the PC. At the rear of the PC reverse flow was measured with a maximum velocity of -0.12 U0 at a distance of 0.2Dpc from rear edge of the PC. The u component takes its minimum value (about -0.2 U0) in the wake of the column at a distance of about 0.8Dc from the rear face of the column. The vertical velocity w is positive (upward) as the flow leaves the scour hole (Figs. 5a and 6). This upflow counteracts the generally downward flow some distance behind the pier so that only a small region with downward flow remains in the SB case while this flow is predominant in the FB case. The flow directly behind the PC and in the interaction region with the column is very complex with various vortices appearing (see blow ups in Fig. 6). The upward flow leaving the SH in the SB case and the gap in the FB case meet the downward flow mentioned above, generating a vortex with anti-clockwise rotation near the bottom corner of the PC. This is much stronger in the

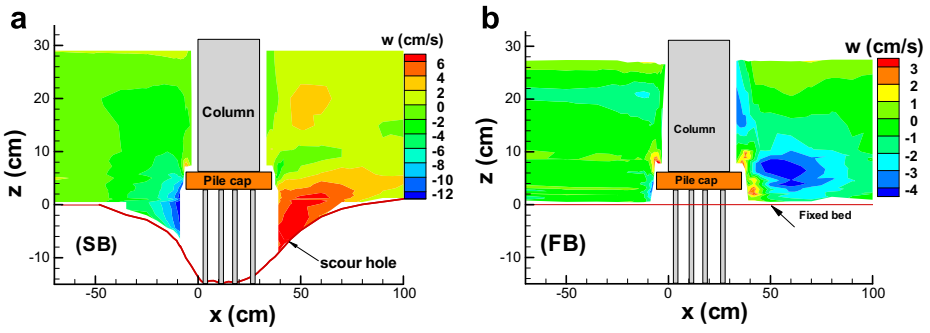

Fig. 5 Velocity contours of w component in the vertical symmetry plane y=0 for SB (**a**) and FB (**b**) cases. Note the different scaling for the SB and FB cases

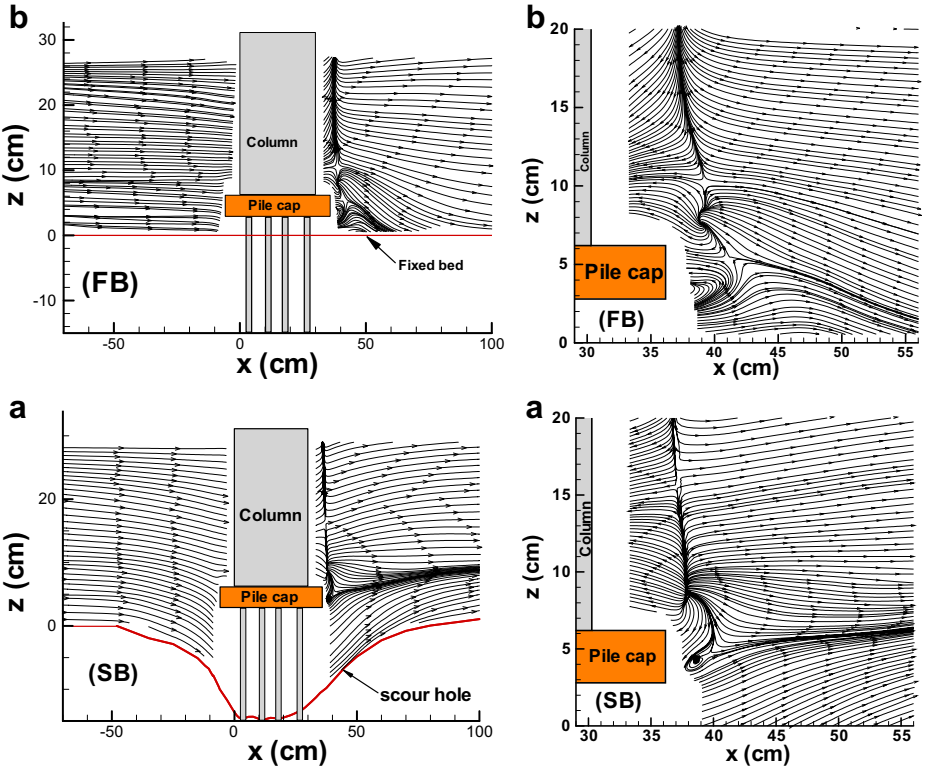

Fig. 6 Streamlines in the vertical symmetry plane y=0 (*left*) and zoomed into the downstream (*near wake*) region (*right*) for SB (**a**) and FB (**b**) cases

FB case, probably because of the stronger downflow. Further up, in the interaction region of PC and column, a counter-rotating vortex develops, primarily due to the back flow at the rear of the PC.

3.1.2 Flow pattern in horizontal planes

Figure 7 compares the contour plots of u for the SB and FB cases in three horizontal planes situated close to the initial bed level [plane z/h = 0.035 (z=1.05 cm), Fig. 7a], mid of the PC [plane z/h= 0.167(z=5.02 cm), Fig. 7b], and above the PC [plane z/h= 0.298 (z=8.97 cm), Fig. 7c]. To clearly show the detailed flow field around the CBP, the contour plots are confined to the region close to the pier. It was noted that in the upstream region below the PC (plane z=1.05 cm), the magnitude of u increases approaching the SH region due to an increase in distance from local bed level in contrast to the FB case (for which the distance from bed is constant z=1.05 cm), and the acceleration of the flow below the PC toward the piles. Then, as indicated it decreases approaching the pier (see Figs. 4 and 7 for SB and FB cases). The maximum value of u at plane z=1.05 cm was measured as about $1.02U_0$along the side of the pier (Fig. 7a). At this plane no reverse flow was observed and u has its minimum value of about $0.4U_0$ in the rear of the pier. This value is larger than for the FB case (Fig. 4a), but the extent of this region of velocity reduction is smaller.

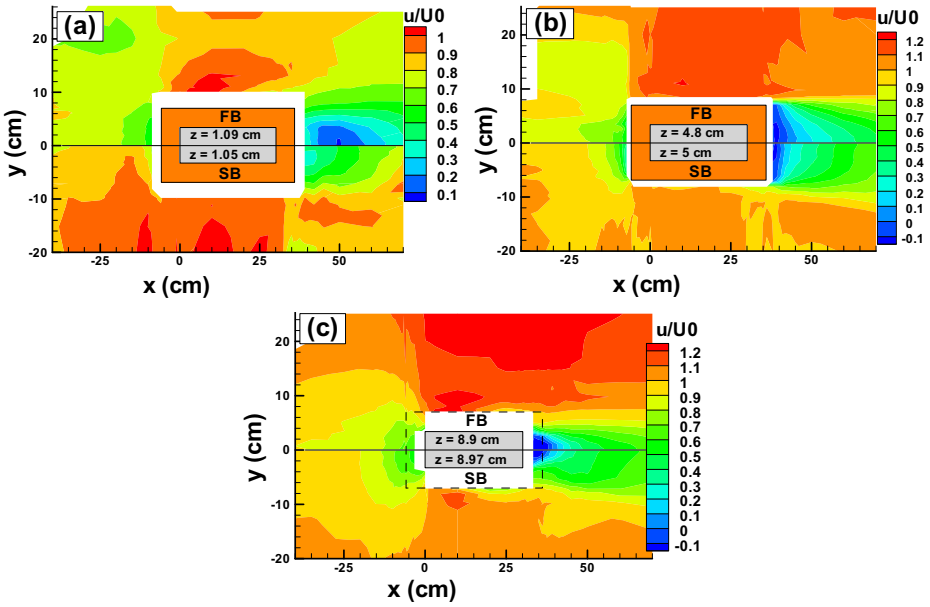

Fig. 7 Comparison of velocity contours of u component at different horizontal planes for fixed bed (FB) and scoured bed (SB) cases

At the plane z=5.02 cm, u reduces substantially in front of the pile cap, while a considerable enhancement of u (about 1.1 U_0) was measured along the side of the PC at about mid length (Fig. 4b). The flow separates from the near edges of the PC and the reverse flow

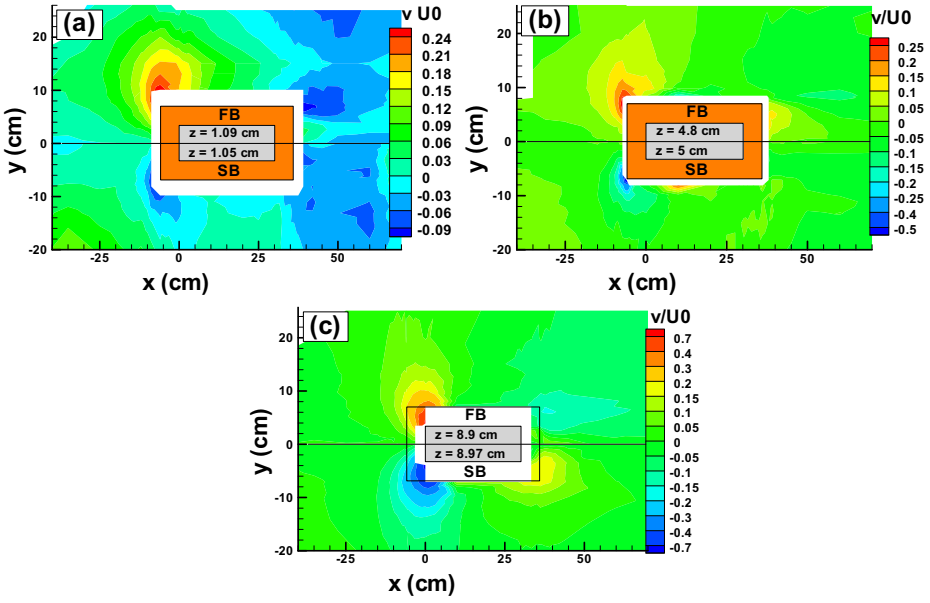

Fig. 8 Comparison of velocity contours of v component at different horizontal planes for fixed bed (FB) and scoured bed (SB) cases

behind the PC (see streamlines in Fig. 9) is fed from the vertical flow in this region (see Fig. 6).

At the plane z=8.97 cm, the variations of u are very similar for the FB and SB cases, especially in the upstream region (see Fig. 7c). In this region, the streamwise velocity decreases approaching the column and takes its maximum values along the sides of the column immediately downstream of the column leading edge at x=0. However, the maximum velocities on the sides of the column are smaller for the SB case than for the FB case. This is due to an increase in flow area as a result of scour development.

In Fig. 8 the contour plots of v are compared for the FB and SB cases at three horizontal planes. For convenience, in this figure the sign of the v is (+) for the FB case and (-) for the scoured bed case. In addition, the streamlines are shown in Fig. 9 for these planes. From Figs. 8a and 9a, it can be seen that even below the PC the presence of the PC deflects the flow sideways, but this deflection is much stronger in the FB case (v_{max} in SB case is only about 30 % of that in FB case). In the FB case this deflected flow is induced by both the flow deflection by the PC front face and the deflection of downward flow at the front of the PC when it reaches the bed, while it is induced only by the former in the SB case. It can be concluded that in the region below the PC the deflected flow is diminished by development of the SH (or by increasing of the PC elevation such that the downward flow at the front of the PC cannot reach the bed). In the upstream region along the SH edges, the flow is deflected slightly toward the hole with $v_{max} \approx 0.12U_0$.

At the plane z = 5.02 cm, the contours of v have similar patterns for the SB and FB-cases, but the maximum values for SB are larger than for FB (see Fig. 8b). The maximum transverse velocity toward the sides of the PC was measured at the upstream corner of the PC and its value is about -0.6U_0. The PC causes the flow to separate at its front

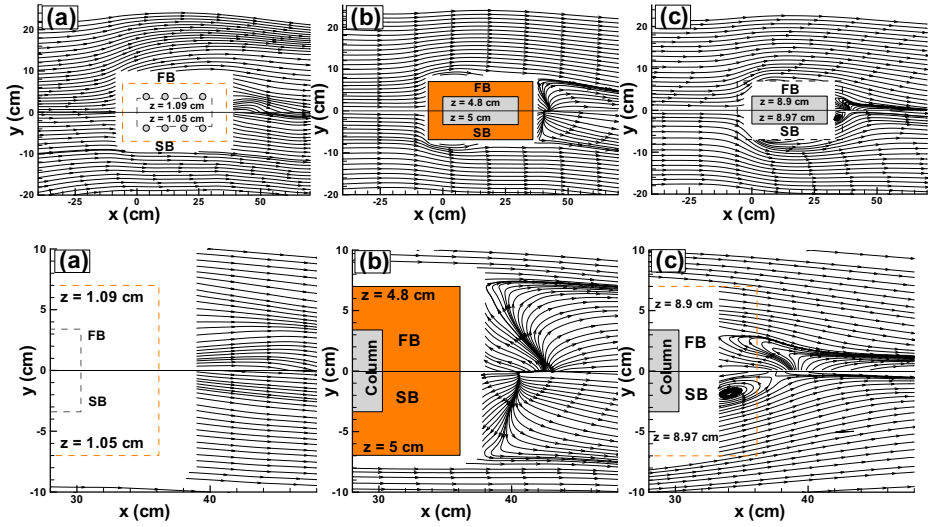

Fig. 9 Streamlines (*top* figures) obtained from velocity fields at horizontal planes, z= 1.05 cm (**a**), z= 5.02 cm (**b**), and z= 8.97 cm (**c**), and zoomed into the downstream (*near wake*) region (*bottom* figures) for scoured bed case (y<0). The results of the flat bed case (at nearly same planes are presented also (y>0) for comparison

corners (barely visible in Fig. 8b), with reattachment at the mid position of the PC. In this reattachment region v is towards the PC with a maximum value of $\approx 0.17U_0$. The vortex (with vertical axis) associated with the separation on the side of the PC is difficult to see within the measurement region due to limitations of the experimental device (see the streamlines in Fig. 9b).

At the plane z = 8. 97 cm, the patterns of flow deflection at the front of the column are also similar for the FB and SB cases (Fig. 8c). A strongly deflected flow was measured at the upstream corner of the column with $v_{max} \approx -0.8U_0$, which is caused mainly by the flow deflection by the column. At the downstream corner of the column, a relatively weak flow ($v_{max} \approx 0.2U_0$) toward the wake region was measured while the flow direction is outward near the bed level at the plane z=1.05 cm (Fig. 8a). These results show that the patterns of the transverse velocity contours at the elevations mid and above the PC remain reasonably unchanged with the presence of the SH (or increasing of the PC elevation).

Moreover, examining the contours in Figs. 7 and 8 and the streamlines in the horizontal planes in Fig. 9 reveals the flow separation associated with flow reversal at the elevations mid and above the PC. Figure 9 shows that the flow in a horizontal plane near the initial bed level is almost unidirectional for the FB case. From this figure it can be seen that the extent of the separated-flow regions in the rear of the PC and column in the presence of a SH is smaller than in the FB case. The extent of the separated-flow region at the rear of the PC is about 1.4 times larger for the fixed bed (FB) compared with the scoured bed (SB) case. Considering the local elevation of the PC (position of the PC with respect to the scoured bed level in the SB case and its position with respect to the initial bed level in the FB case), it can be concluded that the extent of separated-flow produced at the rear of the PC decreases as Y increases (see Fig. 9). Hence, the presence of the SH plays an important role in this flow pattern.

Figure 10 represents the contours of the time-averaged vertical velocity, w, at different horizontal planes for both FB and SB cases. At the plane z= 1.05 cm, the values of w in the SB case are larger than in the flat-bed case due to the presence of the SH (Fig. 10a). At the plane z= 5.02 cm, though the effect of the SH is still evident, especially in the upstream region, the pattern on the side of the PC is similar in both cases (see Fig. 10b). The maximum downward flow was measured as about $-0.5U_0$ along the side of the PC just downstream of the column leading edge and is about 1.5 times that of the corresponding value measured in the FB case. The downward flow in front of the column is completely deflected in the transverse direction after having reached the top surface of the PC and produced a down-flow along the sides of the PC (see Fig. 10b). Moving downstream along the sides of the PC, the$w$ component changes its direction such that there exists an upward flow at the rear of the PC near the downstream edge of it (see also streamlines in Fig. 11). At the plane z= 8.97 cm, the pattern is similar to that of the z= 5.02 cm plane, and the maximum value of w was measured as about $-0.65U_0$ along the sides of the PC (Fig. 10c).

Finally, the streamlines and w contours at different cross sections x= -6 cm, x= 0, x= 33.3 cm, and x= 42 cm are plotted in Fig. 11. Considering the streamlines and w contours at sections x= -6 and 0 cm (see Figs. 11a and b), it is clear that there is a downward flow into the scour hole in this region. At cross sections x= 33.3 and 42 cm (Fig. 11c and d) there is an upward flow leaving the scour hole which, when it encounters the PC, separates at its upper edge and forms a clockwise-rotating streamwise vortex on top of it. These results show that the flow at the rear of the PC is extremely complex, as multiple vortices exist with axes in all three directions.

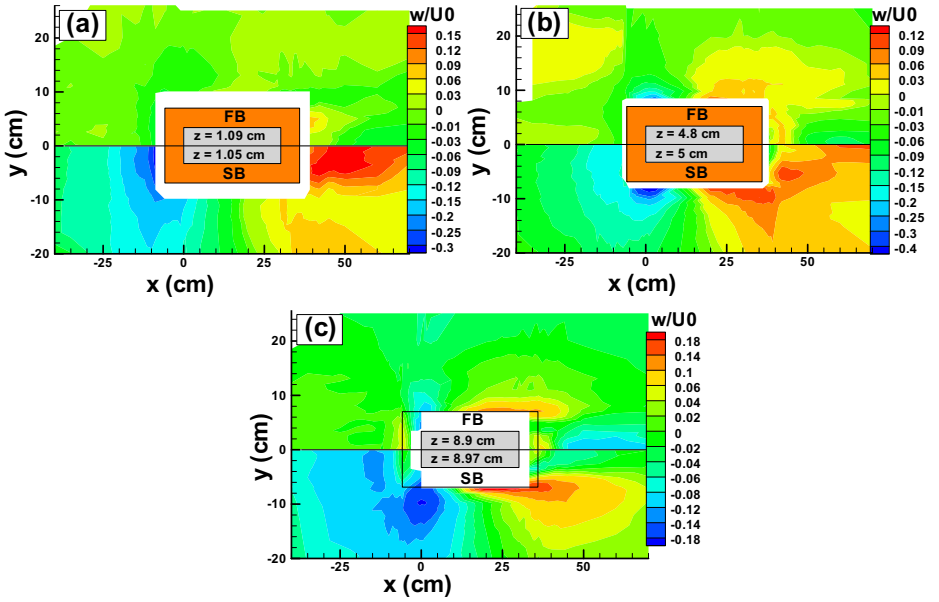

Fig. 10 Comparison of velocity contours of w component at different horizontal planes for fixed bed (FB) and scoured bed (SB) cases

3.2 Turbulent characteristics

3.2.1 Turbulence spectra

Power spectrum analysis of the velocity measurements at different points in the wake of the pier elements was performed in order to find the shedding frequency of the large scale

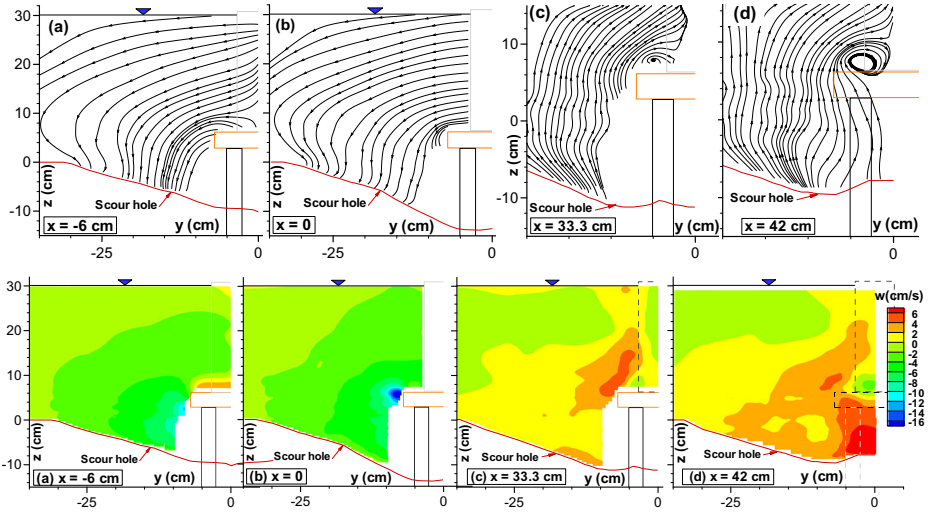

Fig. 11 Streamlines obtained from velocity field (*top* part) and w contours (*bottom* part) at cross sections x=-6, 0, 33.3, and 42 cm

coherent structures in the wake of the pier elements (column, PC, and possibly piles). The power spectra ($S(f) = \{S_u(f)^2 + S_v(f)^2 + S_w(f)^2\}^{0.5}$, cm^2/s) at different points located downstream of the pier are shown in Fig. 12 for the FB case (FB) and the SB case (SB). Here $S_u(f)$, $S_v(f)$, and $S_w(f)$ are power spectra for streamwise, transverse, and vertical velocity components, respectively. The frequencies correspond to the formation of the wake vortices behind each element of the CBP. The peak in the spectra is considered as an indicator of the vortex shedding from the column at points located above the PC (y=10.5 cm, about 4.35 cm above the top of the PC) and from the PC at points located near the mid of the PC (y=4.77 for FB or 5.03 cm for SB). Additionally, the shedding frequency in the wake of the column can be found from spectra plots just behind the column above the PC (Fig. 12, point (x,y,z)= (33.3, -3.4, 15) cm). As can be seen from this figure, the frequency of vortex shedding is $\approx$ 1.2 Hz. The data in Fig. 12 reveal that the frequency of shedding in the wake of the column for the FB case is smaller, while the vorticity strength of the shedding vortices is larger than that of the SB case. Furthermore, the spectra plots for the SB case suggest the absence of well organized, large-scale shedding behind the PC, as can be observed for the

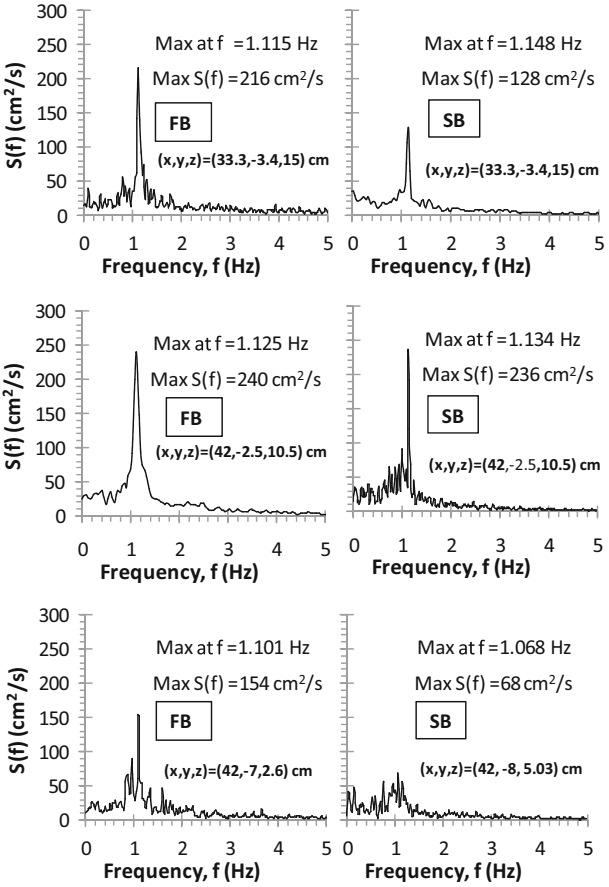

Fig. 12 Power-spectrum, $S(f) = \{S_u(f)^2 + S_v(f)^2 + S_w(f)^2\}^{0.5}$, plots of velocity measurements at the wake region of column and pile cap for flat-bed (FB) and scoured-bed (SB) cases

FB case. This can be attributed to the presence of the SH and the resulting upward motion toward the PC position, which weakened the strength of vorticity of the wake vortices. The power associated with the peak frequency for the power spectrum distribution indicates the strength of vorticity of wake vortices formed by the pier elements. In turn, the strength of wake vorticity expresses the capacity of wake vortices to entrain and move bed sediment from the flanks and rear of the pier [30]. Moreover, spectral analysis for all measured points in the wake of the pier showed that the position of the point at which the maximum power in the wake of the pier was measured is shifted toward the center line for the SB case. This is consistent with the conclusion made in the previous section on the size and extent of the wake vortices behind the pier.

The Strouhal number ($S_t = fD/U$) corresponding to the peak frequencies was calculated to be about 0.2 for the column and about 0.4 for the PC. The Strouhal number describes the vortex shedding frequency for a given velocity (U) and pier diameter (D). The Strouhal number has been shown to be on the order of 0.2 for cylinders of a Reynolds number of 1×10^5 [31]. Ataie-Ashtiani and and Aslani-Kordkandi [14, 15] found Strouhal numbers in the ranges of 0.11 to 0.22 for the cases of single, tandem and side-by-side double piers with Reynolds numbers of 3×10^4 based on the pier diameter, and 10^5 based on the flow depth. However, the Strouhal number calculated for the PC is about two times that commonly value found in cylinder cases. The PC considered here is supported by piles and does not obstruct the full depth of the flow. Both these deviations from the ideal case (a cylinder fully obstructing the flow) can somewhat affect the shedding frequency and hence S_t. Hence, a direct comparison of St between the PC and a free-cylinder case appears not appropriate. These results show that the flow around a PC is different from that of a single uniformly shaped pier, and this effect should be taken into account in calculations of the equivalent diameter of CBPs when estimating the scour depths. In other words, the interaction between different elements of the CBP produce a complex flow pattern and the resulting scour depth could not be calculated by the method of superposition, a method that was used by Richardson and Davis [32] in HEC-18 and by Sheppard and Glasser [18]. To consider the effect of this complex flow on the scour development, it is required that the experiments in the presence of all components of the complex piers be conducted. It is also suggested that the studies of local scour around CBPs based on the separation of pier elements and conducting local scour experiments for each separated element may not be realistic for hydrodynamic considerations, as was done by Sheppard and Jones (see [33]). Instead, in order to take into account the complexity of this flow field around pier elements, especially around the PC, and theirs effects on the resulting scour depth, it is suggested that the local scour studies be done based on dimensional analysis and experiments carried out on piers with all of the components obstructing the flow, as was done by Coleman [16] and Ataie-Ashtiani et al. [17].

3.2.2 Turbulent intensities

The contours of the TIs u^+, v^+, and w^+ at different horizontal planes and vertical sections are presented in Figs. 13, 14, and 15, respectively. It is noted that at the plane z =1.05 *cm*, the distributions of u^+ and v^+ are similar, especially behind the pier. The maximum values of u^+, v^+, and w^+ at plane z= 1.05 cm were measured downstream along the line passing the side position of the PC. The extent of this region with high values of u^+ and v^+ is smaller than that of the FB case [22], while it is larger for w^+. Moreover, there are cores of relatively high v^+ along the side edge of the SH. The amplification of turbulence along the sides of the PC can lead to a mechanism for sediment entrainment in these regions, even if

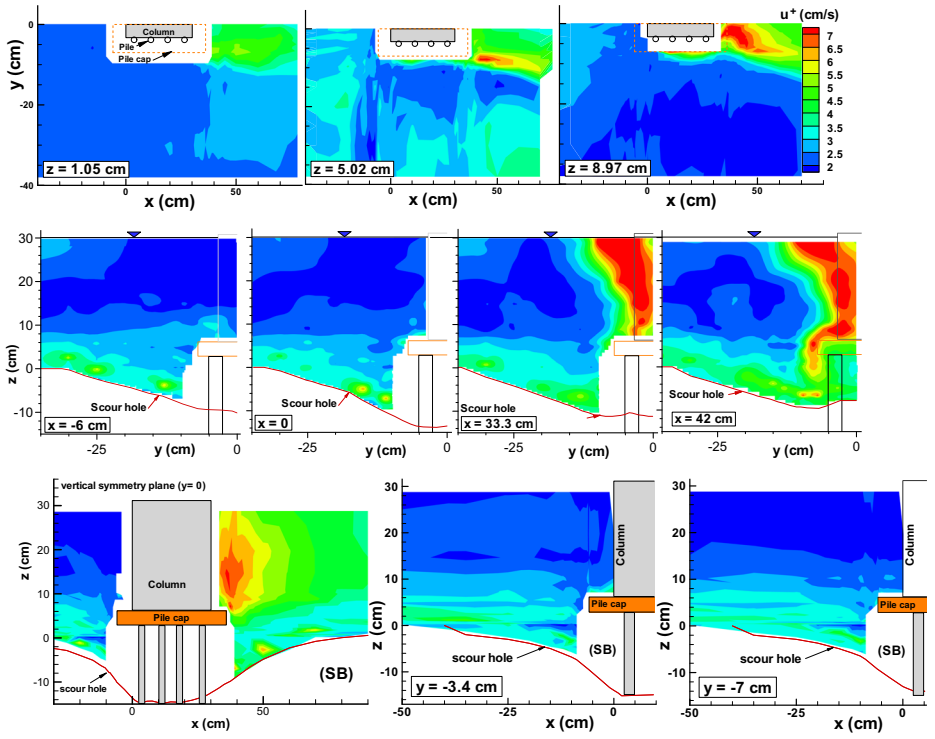

Fig. 13 Contours of u$^+$ (cm/s) at different horizontal planes and vertical sections

the mean shear stresses would be below the critical values [34]. The TIs at the upstream and side of the pier are insignificant at this plane, compared to those of the FB case.

For the plane z =5.02 *cm*, the regions of maximum TIs are observed downstream of and along the side of the PC. For u+ and v+ the regions of highest Tis is in the shear layer springing off the corner of the PC, while for w+ it is close to the plane of symmetry. A comparison between the FB and SB cases shows that the size of these regions of high u^+ and v^+ is smaller for SB, while the size of the region with high w^+ is larger than that of the FB case. At this plane, the TIs along the side of the PC near the mid length of it are also considerable.

At the plane z = 8.97 *cm*, the high levels of turbulence are situated in the wake of the column above the downstream edge of the PC, with maximum values smaller than those of the FB case [22]. Further, in comparison to the FB case, the TIs are relatively high along the side of the pier. Maximum value of w^+ was measured along the PC side, where, from the velocity contours, it can be observed that there exists an upward flow (see Fig. 10c). Upstream of and along the sides of the pier there are some regions of high turbulence inside the SH (see contours of u+ and v+ at cross section planes of x= -6 cm and x=0 in Figs. 13 and 14). The values of u^+ and v^+ are significantly larger (by about one to three orders of magnitude) than the values of w^+. However, in the downstream region the patterns are similar for all components. In the SH region just upstream of the PC, the values of TI first decrease with increasing distance from the bed and reach low values but then increase again toward the PC edges (see the vertical symmetry plane y=0 in Figs. 13 and 14). The

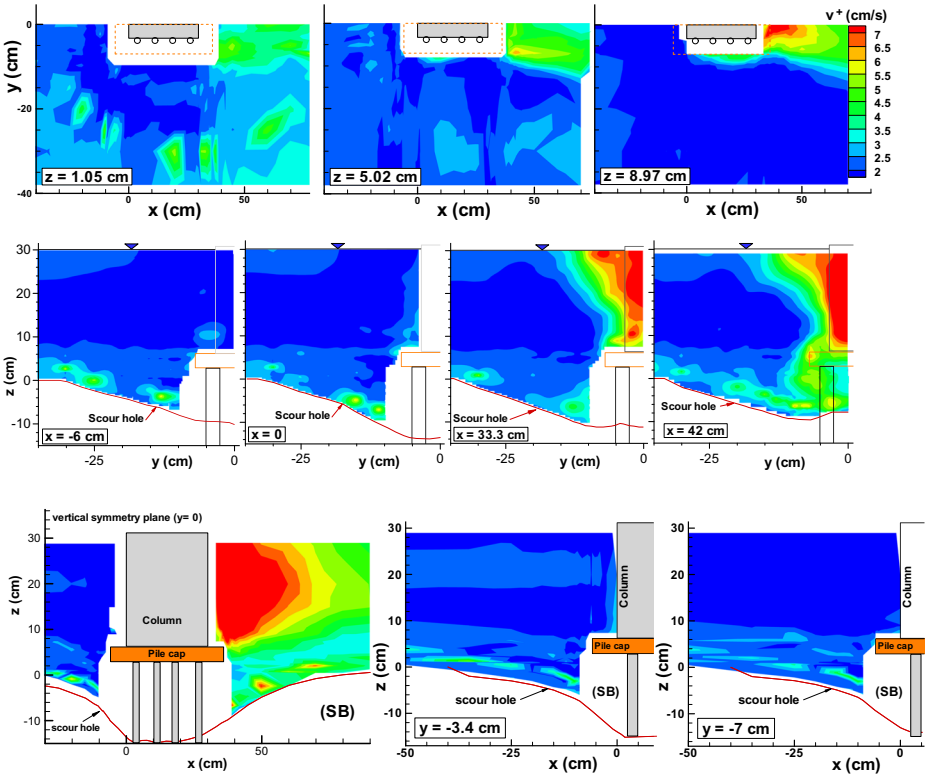

Fig. 14 Contours of v+ (cm/s) at different horizontal planes and vertical sections

highest values are observed only for measured points in the wake of the column above the PC and near its downstream edge at an elevation of about z ≈ 0.5h (z= 15 cm) from initial bed level. In the wake of the pier, the values of the TIs are several orders of magnitude larger than the upstream values. In general, the high values of TIs around the PC reveal the complexity of the flow around it.

The distributions of K, whose contours at different cross sections and in the vertical symmetry plane y= 0 are shown for the SB case in Fig. 16, are similar to those of the TIs. The high levels of K inside the SH along the side of the pier (see cross sections x = 0 and -6 *cm*) characterize the vortical flow pattern at this region. The maximum value of K measured in the wake of the column is more than 2.0 times that inside the SH. For the FB case, the size of the high core of K as well as the maximum values behind the column are larger than those in the SB case shown in Fig. 16 (cross section x= 42 cm and plane y=0).

3.2.3 Reynolds shear stresses

Some of the Reynolds shear stress results (divided by minus of the mass density of water, -ρ), $\overline{u'v'}$, $\overline{u'w'}$, and $\overline{v'w'}$ are shown in Fig. 17 (horizontal plane z= 1.05 cm) and Fig. 18 (vertical symmetry plane) and additional results, which will also be discussed briefly, are

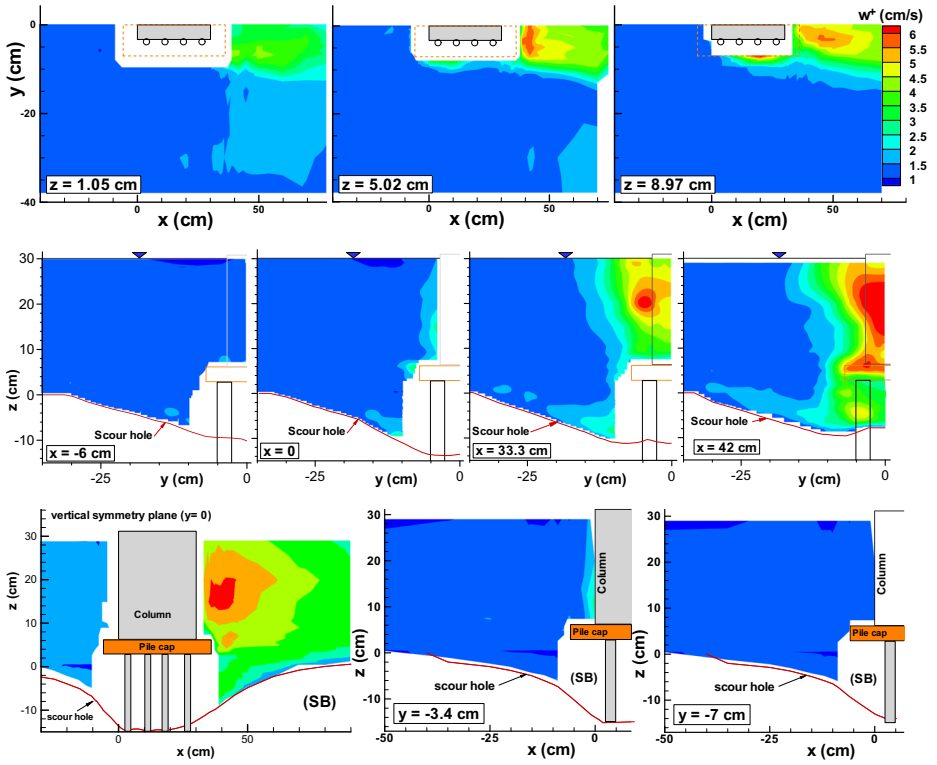

Fig. 15 Contours of w+ (cm/s) at different horizontal planes and vertical sections

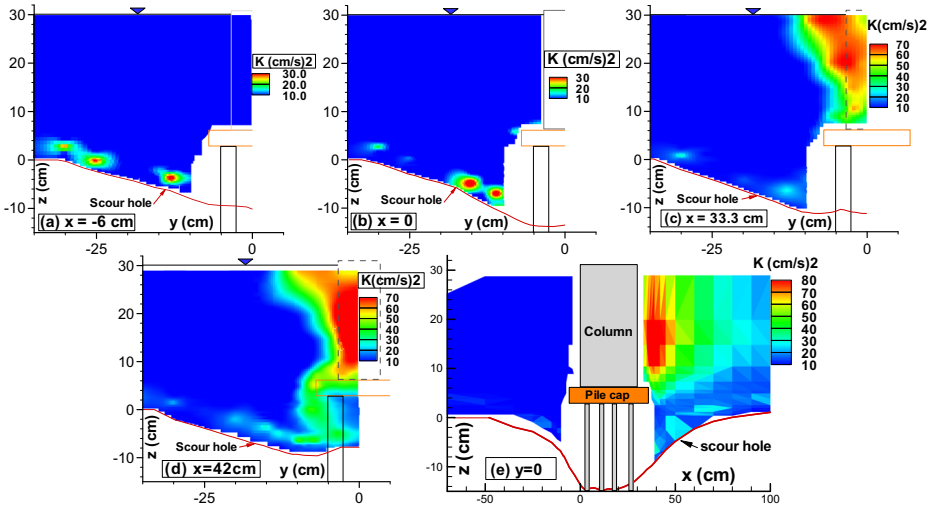

Fig. 16 Contours of K $(cm/s)^2$ at cross sections x= -6 cm (**a**), x= 0 (**b**), x= 33.3 cm (**c**), x= 42 cm (**d**), and vertical symmetry plane y= 0 (**e**)

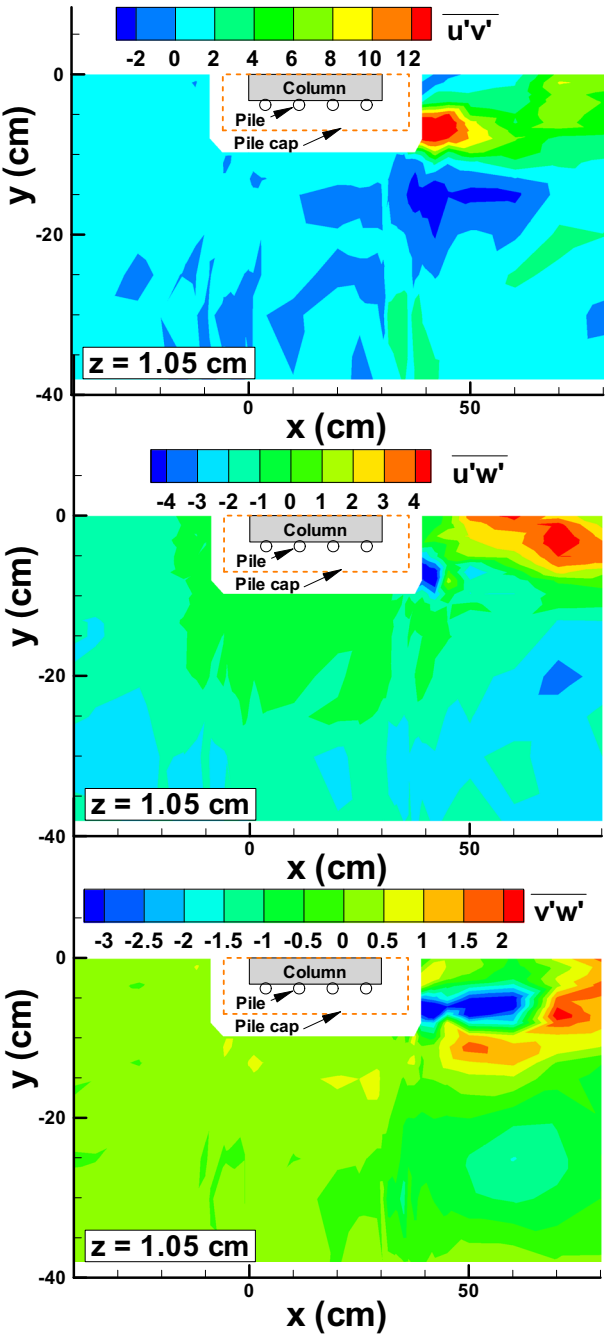

Fig. 17 The contours of the Reynolds shear stresses $\overline{u'v'}$, $\overline{u'w'}$, and $\overline{v'w'}$ $(\mathrm{cm/s})^2$ at the horizontal plane z= 1.05 cm situated close to the initial bed level

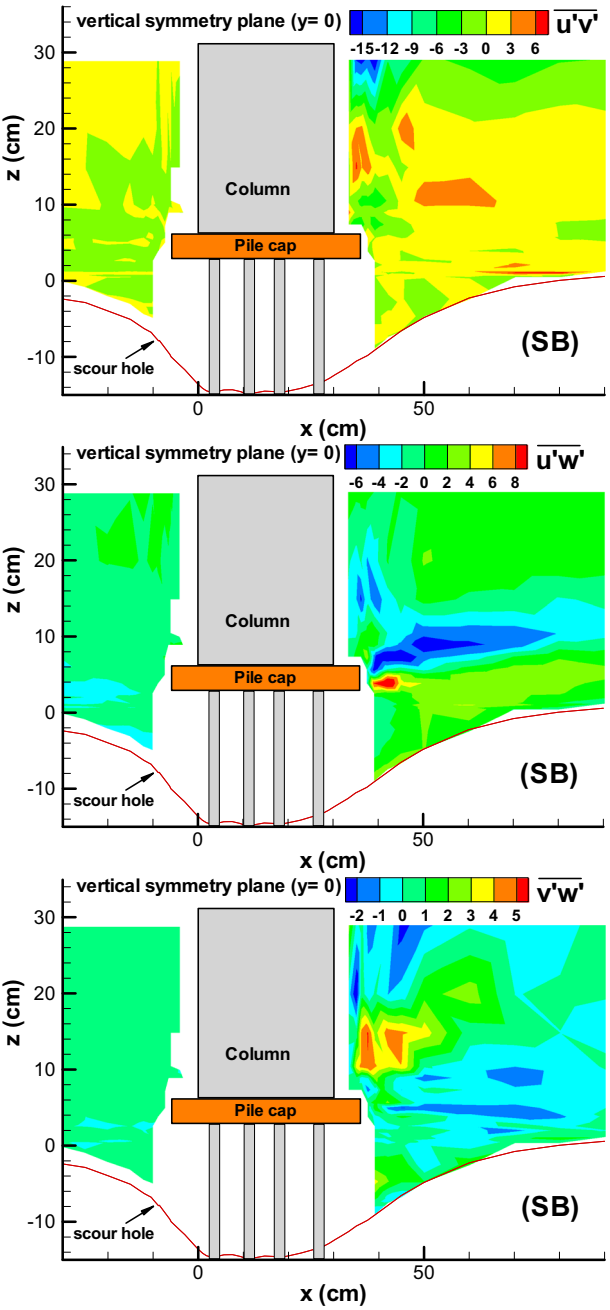

Fig. 18 The contours of the Reynolds shear stresses $\overline{u'v'}$, $\overline{u'w'}$, and $\overline{v'w'}$ $(\text{cm/s})^2$ in the vertical symmetry plane y=0

available as supplementary files that can be obtained at request from the first author. The contours show that the maximum (positive) values of $\overline{u'v'}$ at the planes z=1.05 and 5.02 cm were measured in the shear layers springing off the downstream corners of the PC, while

for the plane z= 8.97 cm the maximum values were measured at the rear of the column. At the plane z=1.05 cm (see Fig. 17), $\overline{u'v'}$ changes sign on both sides of the positive core at the rear of the PC. The values of $\overline{u'v'}$ in the downstream region are more than 10 times the values in the upstream region due to the turbulent mixing of fluid as a result of vortical flow in the rear of the pier. The values of $\overline{u'w'}$ are negative in the shear layer downstream of the PC for plane z=1.05 cm, while for plane z=5.02 cm they change sign from negative along the sides of the PC to positive toward the near-wake region. At the two planes z=1.05 and 5.02 cm, there is also a core of high (positive) $\overline{u'w'}$ at a distance $2.4D_{pc}$ (=33.85 cm) downstream the edge of the PC. At the plane z=8.97 cm, the values of $\overline{u'w'}$ are negative for the majority of points, and the maximum (negative) value, which is the highest measured value, was obtained in the shear layer springing off the edge of the column at a distance of about $2.2D_c$ (=15 cm) downstream of this edge. In the upstream region and near the base of the SH there is a core of high (negative) $\overline{u'w'}$, the size of which decreases toward the side of the pier, while the maximum (negative) value of $\overline{u'w'}$in the core increases. The values of $\overline{u'w'}$ increase when approaching the piles inside the SH, probably due to the effect of the piles. In the downstream region, the contours of $\overline{u'w'}$ indicate a complex vortical flow in the rear of the PC, as the values change sign from positive (near the bottom corner of the PC) to negative (near top corner of the PC) (see Fig. 18). The highest (positive and negative) values of $\overline{u'w'}$ were measured at cross section x=42 cm at an elevation near to the PC position. The values of $\overline{v'w'}$ are generally lower than those of the other two components, the contours showing a complex pattern in the rear of the column and around the PC.

4 Conclusions

The turbulent flow field around a complex bridge pier with a developed scour hole was studied by measuring instantaneous velocities using ADV. Using the time-averaged velocities, TIs, and Reynolds shear stresses at different horizontal planes and at different longitudinal and cross sections , the following major conclusions are derived.

Upstream of the pier no reversal of flow was observed and hence also no horseshoe vortex because the flow near the bed could pass underneath the main obstructing parts of the CBP, especially in the SB case with significant SH. The flow approaching the PC was diverted by this upward and downward and also around the sides where it separated but reattached midway along the PC sides. The flow approaching the column was also generally deflected downward because of the gap/scour hole below the PC; it was then deflected sideways by the top surface of the PC and then downward again when flowing around the side faces of the PC. Depending on the PC elevation, the overall downward flow in this front region can reach the bed and erode the bed materials. With development of the SH (or equivalently increasing the PC elevation) this effect diminishes and the flow around the piles may become dominant.

In the downstream region, a multi-compound flow structure is observed, especially close to the PC position. Starting from the water surface, there is a region of reversed flow in the rear of the column which extends in size as one moves toward the PC. Downstream of this region of reversed flow and at some distance above the PC there is a downward flow toward the bed for the FB case. This downward flow overcomes the unidirectional flow near the bed coming from the gap between the piles, and reaches the bed at x$\approx$ 48.5 cm (i.e. about 0.9 D_{pc} or equivalently 2Y from the downstream edge of the PC), where the velocity has a very small magnitude. With developing SH, this downward flow is largely over ruled by the upward flow induced in the SH. In both cases, there is an upward flow near the bottom

corner of the PC toward its top. This upward flow interacts with the downward flow near the top of the PC thereby inducing a vortex near the bottom corner. Further up, near the top corner of the PC, due to the reverse flow behind the PC a secondary vortex develops with a sense of rotation opposite to that of the first vortex near the bottom corner of the PC. With developing SH the upward flow below the PC is enhanced and the downward flow region is limited to the region very close to the PC; this in turn results in an enlargement of the size of the secondary vortex near the top corner of the PC, while the vortex near the bottom corner dwindles in size. The streamlines in the horizontal planes revealed that the extension of the separation region in the rear of the PC and column is smaller in the SB than in the FB case. Further downstream of the pier at cross sections x = 33.3 and 42 *cm*, small streamwise rollers (clockwise rotation looking upstream) were formed at an elevation near the top corner of the PC. The complexity of flow behind the PC is the main reason for the amplification of turbulence in this region, identifying a mechanism for sediment entrainment around the pier.

Spectral analysis has shown larger strength of vorticity of shed vortices from the column for the FB case when compared with the SB case. The spectra plots for the scoured-bed case suggest the absence of well structured, large-scale shedding behind the PC, as a result of the SH and the induced upward motion toward the PC position. Moreover, spectral analysis for all the measured points in the wake of the pier showed that the size and extent of wake vortices behind the pier are smaller than for the FB case.

Overall, the flow around the PC is significantly influenced by the development of the SH, in contrast to the minor influence of the SH on flow around the column. It should be emphasized that some of the conclusions drawn here are observed and presented for the first time and demonstrate the necessity of detailed measurements for the understanding of the flow field around complex bridge piers.

Acknowledgments The authors wish to thank the journal editor Professor Wolfgang Rodi for his thoughtful comments and helpful modifications which helped to improve the final manuscript. Also the anonymous reviewers' constructive comments are appreciated.

Notation

The following symbols *are used in this paper:*

b_p = pile diameter;
Dc = pier column width;
D_{pc} = pile cap width;
d_{50} = mean particle diameter;
d_{se} = equilibrium scour depth;
f = frequency;
G = side to side distance between the piles;
h = approach flow depth;
K =turbulent kinetic energy;
L_c = column length;
L_{pc} = pile cap length;
m = number of piles in line with the flow;
n = number of piles normal to the flow direction;
Ss = specific gravity of sand;
S_t = Strouhal number;
T = pile cap thickness;
U_0 = mean approach velocity;

u, v, w = time averaged velocity in x, y, $z$direction, respectively;
u', v', w' = fluctuating velocity in x, y, $z$direction, respectively;
V = time-averaged absolute velocity;
v_{max} = maximum value of the transverse velocity;
x, y = streamwise, and transverse directions, respectively;
Y = distance from initial bed level to the top of the pile cap;
z = vertical direction and distance above the initial bed;
ρ = fluid density;
σ_g = particle diameter geometric standard deviation.

References

1. Breusers, H.N.C., Niccollet, G., Shen, H.W.: Local scour around cylindrical piles. J. Hydraul. Res. **15**(3), 211–252 (1977)
2. Melville, B.W., Coleman, S.E.: Bridge scour. Water Resources Publications, Colo (2000)
3. Sheppard, D., Max Odeh, M., Glasser, T.: Large Scale Clearwater Local Pier Scour Experiments. J. Hydraul. Eng. ASCE **114**(10), 1210–1226 (2004)
4. Dargahi, B.: Controlling mechanism of local scouring. J. Hydraul. Eng. ASCE **116**(10), 1197–1214 (1990)
5. Kirkil, G., Constantinescu, S.G., Ettema, R.: Coherent structures in the flow field around a circular cylinder with scour hole. J. Hydraul. Eng. ASCE **134**(5), 572–587 (2008)
6. Landers, M.N., Mueller, D.S.: Channel scour at bridges in the United States. Pub. FHWA-RD-95-184. USDOT, Turner Fairbanks Hwy. Res. Ctr., McLean, Va (1996)
7. Melville, B.W.: Local scour at bridge sites. Rep. No. 117, School of Engineering, The University of Auckland, New Zealand (1975)
8. Ataie-Ashtiani, B., Beheshti, A.A.: Experimental investigation of clear-water local scour at pile groups. J. Hydraul. Eng. ASCE **132**(10), 1100–1104 (2006)
9. Dey, S., Raikar, R.V.: Characteristics of horseshoe vortex in developing scour holes at piers. J. Hydraul. Eng. ASCE **133**(4), 399–413 (2007)
10. Ahmed, F., Rajaratnam, N.: Flow around bridge piers. J. Hydraul. Eng. ASCE **124**(3), 288–300 (1998)
11. Graf, W.H., Istiarto, I.: Flow pattern in the scour hole around a cylinder. J. Hydraul. Res. **40**(1), 13–20 (2002)
12. Roulund, A., Sumer, B.M., Fredsøe, J., Michelsen, J.: Numerical and experimental investigation of flow and scour around a circular pile. J. Fluid Mech. **534**, 351–401 (2005)
13. Kirkil, G., Constantinescu, G.: Flow and turbulence structure around an in-stream rectangular cylinder with scour hole. Water Resour. Res. **46**(11) (2010). doi:10.1029/2010WR009336
14. Ataie-Ashtiani, B., Aslani-Kordkandi, A.: Flow field around side-by-side piers with and without a scour hole. Eur. J. Mech. B/Fluids **36**, 152–166 (2012)
15. Ataie-Ashtiani, B., Aslani-Kordkandi, A.: Flow Field around Single and Tandem Piers. Flow Turbulence and Combustion **90**(3), 472–490 (2013)
16. Coleman, S.E.: Clearwater local scour at complex piers. J. Hydraul. Eng. ASCE **131**(4), 330–334 (2005)
17. Ataie-Ashtiani, B., Baratian-Ghorghi, Z., Beheshti, A.A.: Experimental investigation of clear-water local scour of compound piers. J. Hydraul. Eng. ASCE **136**(6), 343–51 (2010)
18. Sheppard, D., Max Glasser, T.: Sediment scour at piers with complex geometries. Proceedings of 2nd International Conf. on Scour and Erosion. World Scientific, Singapore (2004)
19. Beale, S.B., Spalding, D.B.: A numerical study of unsteady fluid flow in in-line and staggered tube banks. J. Fluids Struct. **13**, 723–754 (1999)
20. Ge, L., Lee, S.O., Sotiropoulos, F., Sturm, T.: 3D unsteady RANS modeling of complex hydraulic engineering flows. II: model validation and flow physics. J. Hydraul. Eng. ASCE **131**(9), 809–820 (2005)
21. Ge, L., Sotiropoulos, F.: 3D unsteady RANS modeling of complex hydraulic engineering flows. I: numerical model. J. Hydraul. Eng. ASCE **131**(9), 800–808 (2005)
22. Beheshti, A.A., Ataie-Ashtiani, B.: Experimental Study of Three Dimensional Flow Field around a Complex Bridge Pier. J. Eng. Mech. ASCE **136**(2), 143–154 (2010)
23. Kumar, A., Kothyari, U.C.: Three-dimensional flow characteristics within the scour hole around circular uniform and compound piers. J. Hydraul. Eng. ASCE **138**(5), 420–429 (2012)

24. Beheshti, A.A., Ataie-Ashtiani, B.: Analysis of threshold and incipient conditions for sediment movement. Coast. Eng., Int. J. for Coastal, Harbour, Offshore Eng. **55**, 423–430 (2008)
25. NORTEK AS. *ADV operation material.* Nortek AS, Vollen, Norway;1996
26. Wahl, T.L.: Analyzing ADV data using WinADV. Proc., Joint Conf. on Water Resources Engineering and Water Resources Planning and Management, ASCE, Reston, Va (2000)
27. Wahl, L.T.: Discussion of "Despiking Acoustic Doppler Velocimeter data" by D. G. Goring and V. I. Nikora. J. Hydraul. Eng. ASCE **129**(6), 484–487 (2003)
28. Voulgaris, G., Trowbridge, J.: Evaluation of the acoustic doppler velocimeter (ADV) for turbulence measurements. J. Atmos. Ocean Technol. **15**(1), 272–288 (1998)
29. García, C.M., Cantero, M.I., Niño, Y., García, M.H.: Turbulence Measurements with Acoustic Doppler Velocimeters. J. Hydraul. Eng. ASCE **131**(12), 1062–1073 (2005)
30. Ettema, R., Kirkil, G., Muste, M.: Similitude of Large-Scale Turbulence in Experiments on Local Scour at Cylinders. J. Hydraul. Eng. ASCE **132**(1), 33–40 (2006)
31. Schlichting, H. Boundary layer theory, 7th Ed. McGraw-Hill, New York (1979)
32. Richardson, E.V., Davis, S.R.: Evaluating scour at bridges Hydraulic Engineering Circular No. 18 (HEC-18), Rep. No. FHWANHI 01-001. Federal Highway Administration, Washington (2001)
33. Sheppard, D., Max Renna, R.: Florida Bridge Scour Manual. Published by Florida Department of Transportation, 605 Suwannee Street, Tallahassee, FL 32399–0450 (2005)
34. Sumer, B.M., Chua, L.H.C., Cheng, N.S., Fredsøe, J.: Influence of turbulence on bed load sediment transport. J. Hydraul. Eng. ASCE **129**(8), 585–596 (2003)